Supplementary Materials

The Structure of Galactoglucomannan Impacts the Degradation under Alkaline Conditions

Jennie Berglund[1], Shoaib Azhar[2], Martin Lawoko[1], Mikael Lindström[1], Francisco Vilaplana[1,3], Jakob Wohlert[1], Gunnar Henriksson[1*]

[1]Wallenberg Wood Science Centre (WWSC), Department of Fibre and Polymer Technology, School of Engineering Sciences in Chemistry, Biotechnology and Health, KTH Royal Institute of Technology, SE-100 44 Stockholm, Sweden,

[2]AkzoNobel Pulp and Performance Chemicals, SE-85239, Sundsvall, Sweden

[3]Division of Glycoscience, School of Engineering Sciences in Chemistry, Biotechnology and Health, KTH Royal Institute of Technology, AlbaNova University Centre, SE-106 91 Stockholm, Sweden

*E-mail: ghenrik@kth.se

*Phone: +46 8-790 61 63

Hydroxide model

In traditional simulations it is challenging to describe hydroxide ions in a way that reproduce the thermodynamic behavior and correct coordination with surrounding media. Recently a model with polarized charge showed good structural properties using a polarizable force field (Hub, et al., 2014), and this model was later modified into a non-polarizable force field (Wolf, et al., 2014). In this work a similar translation from the polarizable model was made and the parameters used are described in Fig. S1. However, when verifying the coordination numbers with our system the interaction with water was too weak and an unphysical interaction with Na^+ was observed. Therefore, an additional repulsion was added to a level where coordination between O* and Na^+ was avoided, the potentials were $\sigma = 3.5$ Å and $\varepsilon = 0.19694$ kJ/mol. This resulted in a good model and the coordination number between O* and water oxygen was 4.1, which is similar to the value 4.2 observed by neutron scattering of 2M NaOH solution (McLain, et al., 2006) and 4.4 which was obtained in (Hub et al. 2014).

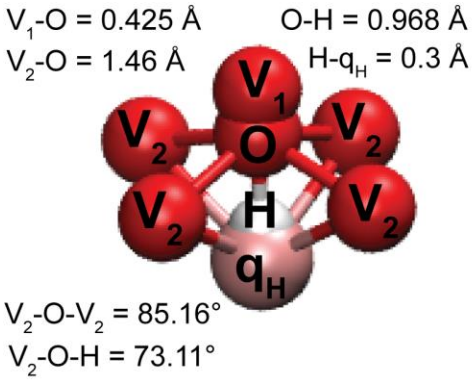

q_O (e)	-1.23
q_H (e)	0.23
ε (kJ/mol)	0.21506
σ_O (Å)	-
σ_{V1} (Å)	2.916
σ_{V2} (Å)	2.5
σ_{HH} (Å)	1.4

Fig. S1 OH-model used in this work, parameters based on previous work (Hub, et al. 2014; Wolf, et al., 2014).

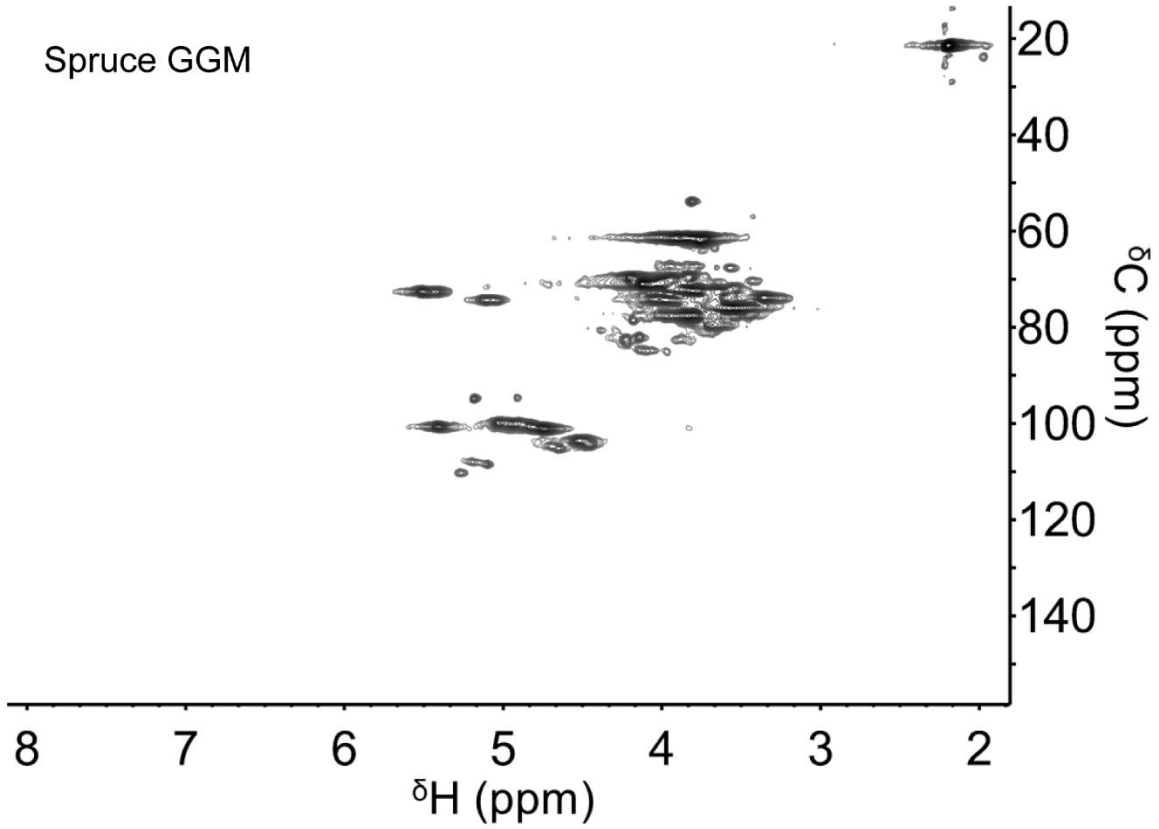

Fig. S2 Full HSQC NMR spectrum of spruce GGM in D_2O.

Table S1 NMR assignments. M=mannose, G=glucose, Gal=galactose, Ara=arabinose. Assignments are made according to earlier work by Hannuksela and Hervé du Penhoat (2004).

	Explanation	**$^{\delta}$H / $^{\delta}$C (ppm)**
M1(int)	C6	4.7 / 101.0
M1$_{M3OAc}$	C1 when C3 is acetylated	4.8 / 100.4
M1$_{M2OAc}$	C1 when C2 is acetylated	4.9 / 100.0
M1$_{\alpha}$(red)	C1 reducing end, α config.	5.2 / 94.8
M1$_{\beta}$(red)	C1 reducing end, β config.	4.9 / 94.6
M2	C2	4.1 / 70.7
M2$_{M3OAc}$	C2 when C3 is acetylated	4.2 / 69.6
M2-OAc	Acetylated C2	5.5 / 72.5
M3	C3	3.8 / 72.2
M3-OAc	Acetylated C3	5.1 / 74.4
M4$_{M2OAc}$	C4 when M2 is acetylated	3.8 / 77.4
M4$_{M3OAc}$	C4 when M3 is acetylated	4.0 / 74.1
M5$_{M2OAc}$	C5 when M2 is acetylated	3.5 / 76.0
M6	C6 (Man and Glc overlap)	3.8 / 61.9
M6$_{M2OAc}$	C6 when C2 is acetylated	3.9 / 67.4
G1(int)	C1 internal	4.5 / 103.8
G2	C2	3.3 / 74.0
G4	C4	3.7 / 80.0
G6	C6 (Man and Glc overlap)	3.8 / 61.9
Gal1$_{\alpha}$(int)	C1 internal, α config.	5.0 / 99.8
Gal1$_{\beta}$(int)	C1 internal, β config.	4.7 / 105.1
Ara1(int)	C1 internal	5.3 / 110.1
Ara2	C2	4.0 / 84.8
Ara3	C3	3.9 / 82.4
Ara4	C4	4.1 / 84.8
OAc	O-acetyl group	2.2 / 21.6
OCH3	Methoxy group	3.8 / 53.8

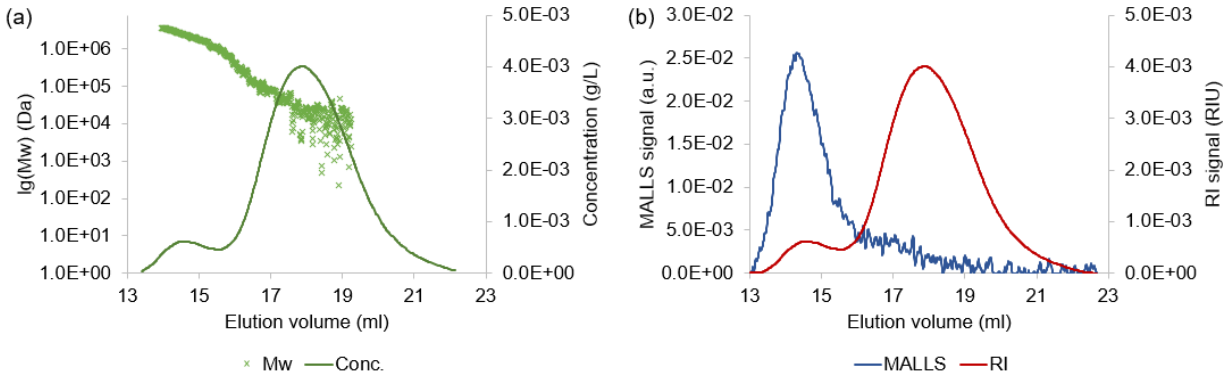

Fig. S3 Molecular weight distribution of spruce GGM determined by SEC-RI-MALLS (eluent DMSO 0.5% LiBr).

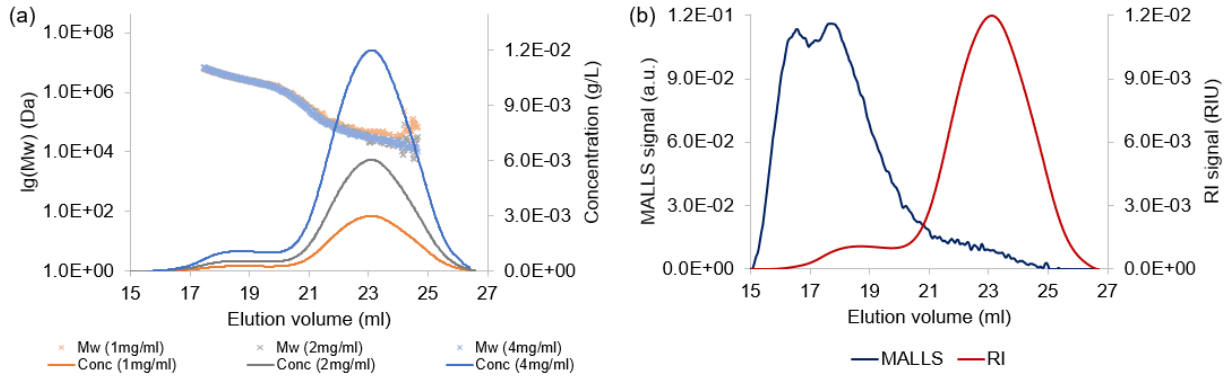

Fig. S4 Molecular weight distribution of spruce GGM determined by SEC-RI-MALLS (eluent 0.1 M $NaNO_3$ and 5 mM NaN_3).

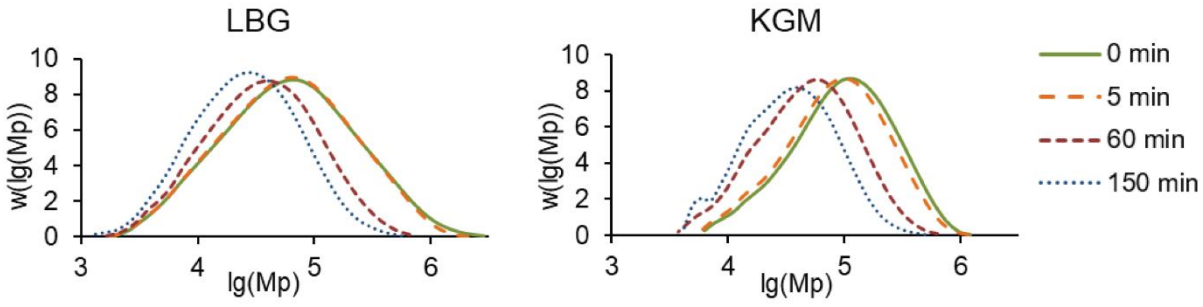

Fig. S5 Molecular weight distributions of LBG and KGM determined by SEC analysis in 10 mM NaOH.

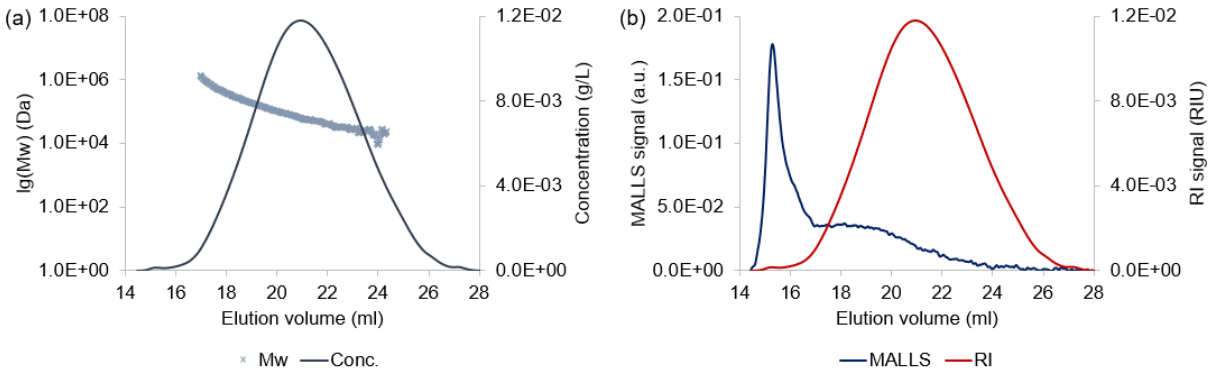

Fig. S6 Molecular weight distribution of LGB determined by SEC-RI-MALLS (eluent 0.1 M $NaNO_3$ and 5 mM NaN_3).

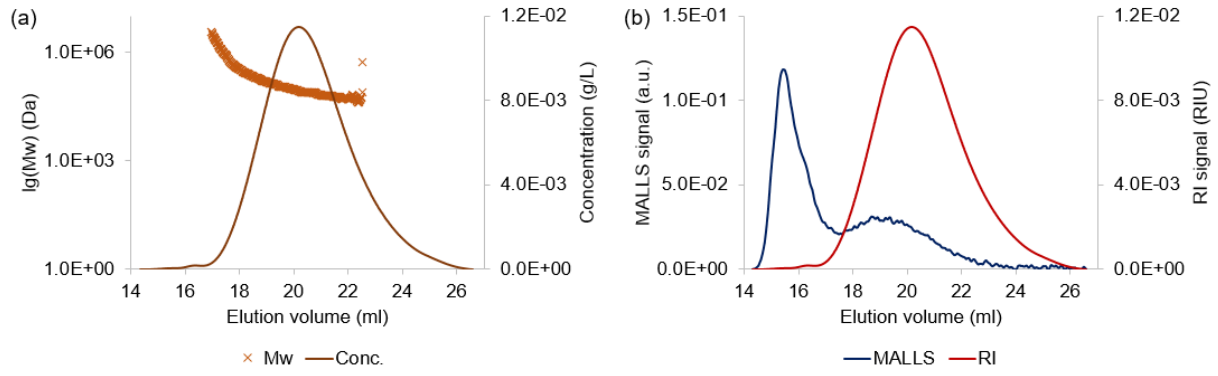

Fig. S7 Molecular weight distribution of KGM determined by SEC-RI-MALLS (eluent 0.1 M $NaNO_3$ and 5 mM NaN_3).

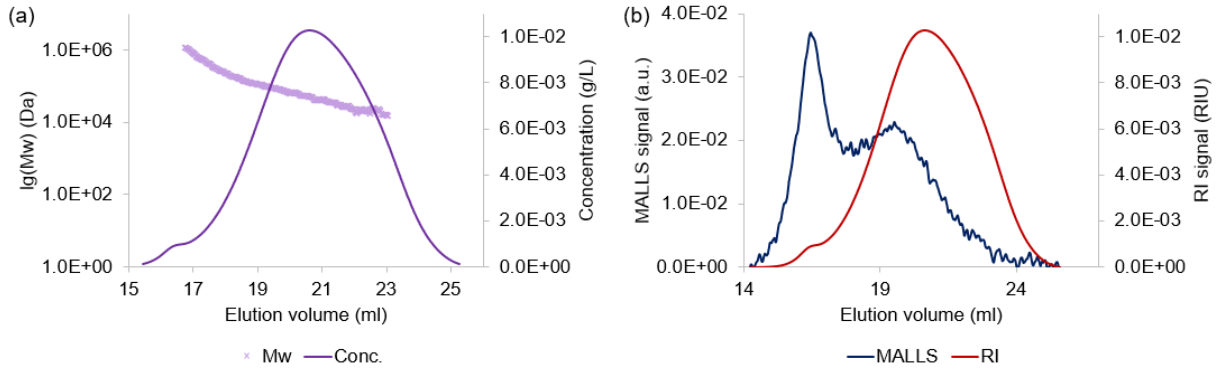

Fig. S8 Molecular weight distribution of CMC determined by SEC-RI-MALLS (eluent 0.1 M $NaNO_3$ and 5 mM NaN_3).

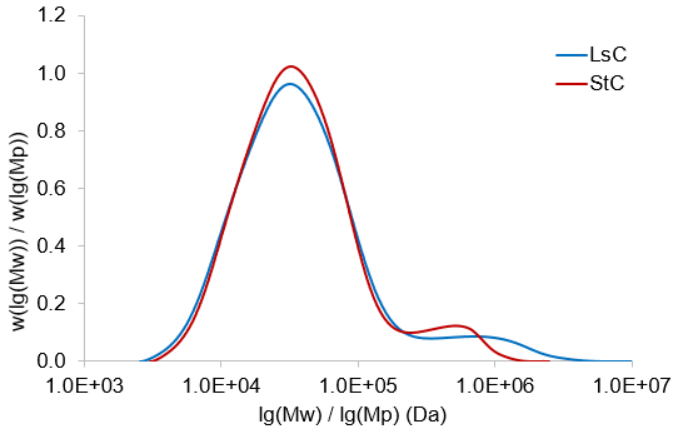

Fig. S9 Molecular weight distribution of spruce GGM determined by SEC with light scattering (LsC) and standard (StC) calibration separately (analyzed by SEC-RI-MALLS with eluent 0.1 M $NaNO_3$ and 5 mM NaN_3).

Table S2 Comparison between Mw calculated by standard calibration (StC) and light scattering (LsC) analyzed in 0.1 M $NaNO_3$ and 5 mM NaN_3.

	Mw StC	**Mw LsC**
GGM-P2	37 100	39 300
GGM-P1	492 900	358 600
LBG	187 300	89 700
KGM	213 100	93 800
CMC	227 300	70 800

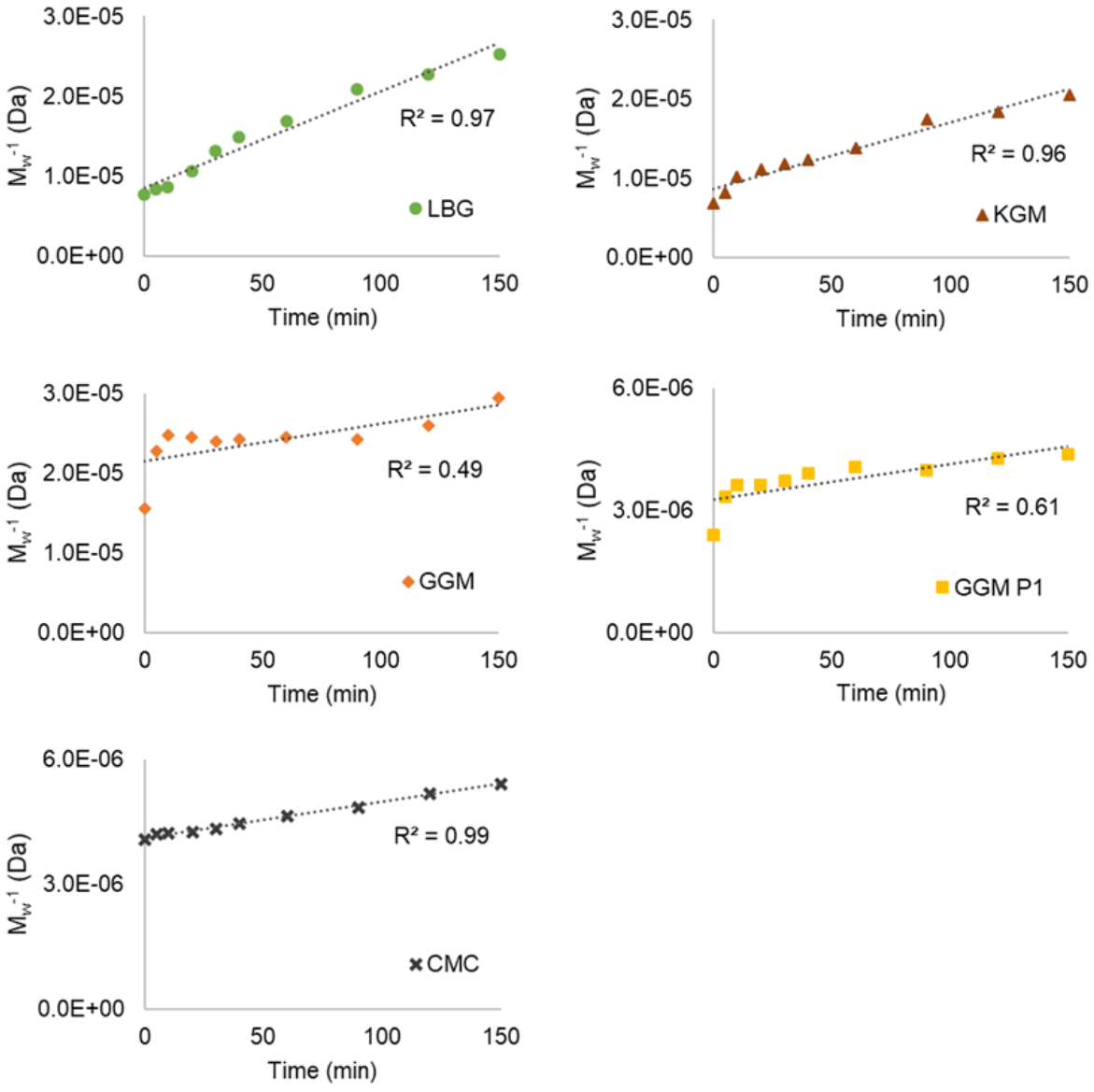

Fig. S10 Analysis of $(Mw)^{-1}$ to time for comparison with the model for random depolymersiation as also perfomed in Pu et al. (2017) comparing to the Malhotra model (Malhotra, 1986).

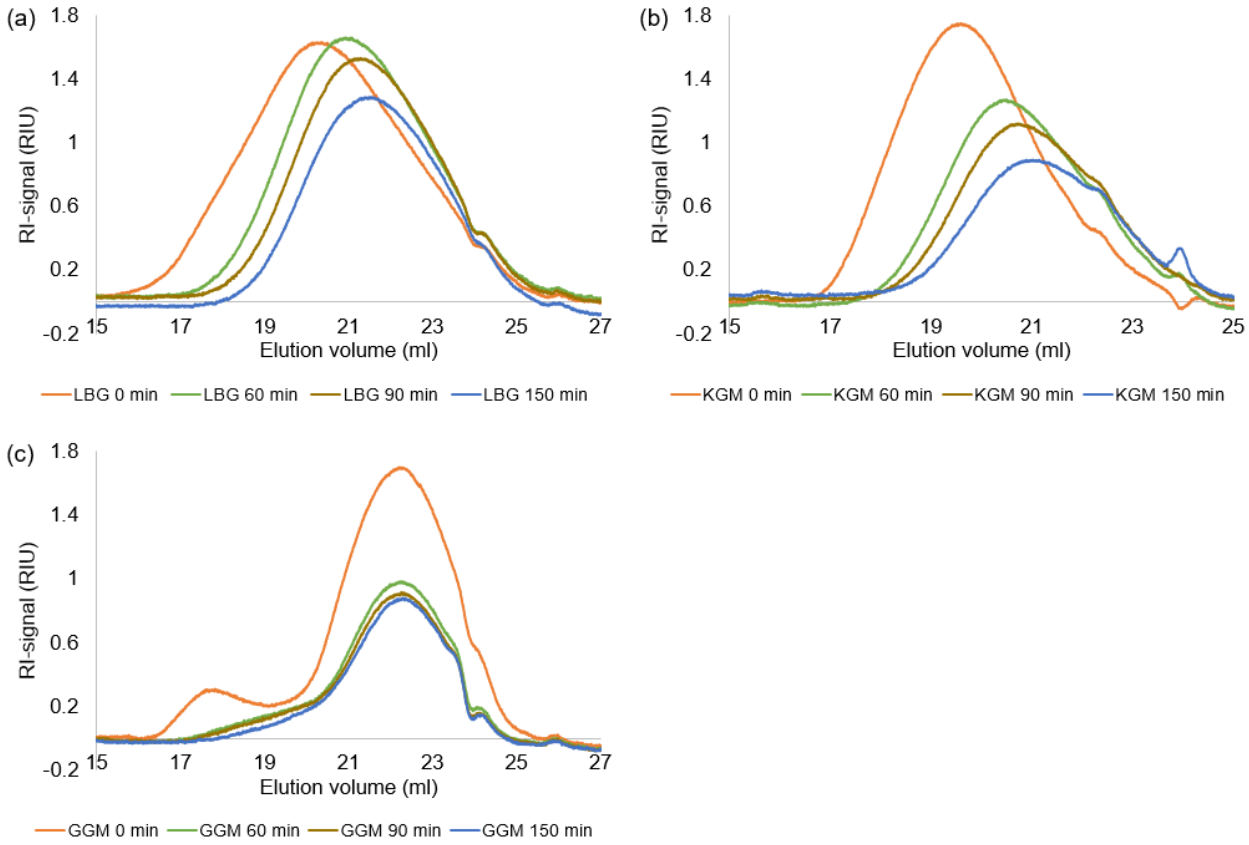

Fig. S11 Raw data of RI-detector responses of (a) LBG, (b) KGM, and (c) GGM in 10 mM NaOH SEC. The RI-signal is concentration dependent and therefore this shows that the yields are decreasing during treatment, however, samples are dialyzed which might alter the concentrations slightly.

Table S3 Sugar composition of the studied mannans given in percent (%) of each sugar.

		Arabinose	Galactose	Glucose	Xylose	Mannose
GGM	0 min	2.9	10.9	27.0	0.7	58.5
	5 min	2.6	9.4	28.0	0.7	59.2
	10 min	2.8	8.5	28.3	0.7	59.7
	20 min	2.9	8.9	29.2	0.8	58.2
	30 min	3.5	9.6	30.2	1.0	55.8
	40 min	3.7	9.4	31.3	1.0	54.6
	60 min	4.1	9.7	32.9	1.2	52.2
	90 min	4.5	10.3	33.4	1.3	50.4
	120 min	4.9	9.7	32.2	1.3	51.9
	150 min	4.8	10.1	33.2	1.3	50.5
LBG	0 min	0.3	20.7	0.7	0.1	78.2
	5 min	0.3	20.4	0.7	0.1	78.5
	10 min	0.3	20.3	0.7	0.1	78.5
	20 min	0.3	19.9	0.7	0.1	79.0
	30 min	0.4	20.2	1.0	0.1	78.3
	40 min	0.4	20.4	1.0	0.1	78.1
	60 min	0.4	20.5	0.8	0.1	78.2
	90 min	0.4	20.3	0.7	0.1	78.5
	120 min	0.4	19.9	0.6	0.1	78.9
	150 min	0.4	20.4	0.7	0.1	78.4
KGM	0 min	0.2	1.2	36.2	0.1	62.3
	5 min	0.3	1.7	36.7	0.2	61.1
	10 min	0.4	1.9	36.8	0.2	60.8
	20 min	0.2	1.5	36.0	0.2	62.1
	30 min	0.3	0.9	35.9	0.2	62.7
	40 min	0.2	1.4	36.4	0.2	61.9
	60 min	0.3	1.8	37.0	0.2	60.7
	90 min	0.2	1.2	36.1	0.3	62.2
	120 min	0.3	1.7	36.7	0.2	61.1
	150 min	0.6	3.1	37.7	0.4	58.2
Standard error ±		0.02-0.40	0.02-0.82	0.02-0.91	0.01-0.17	0.14-2.08

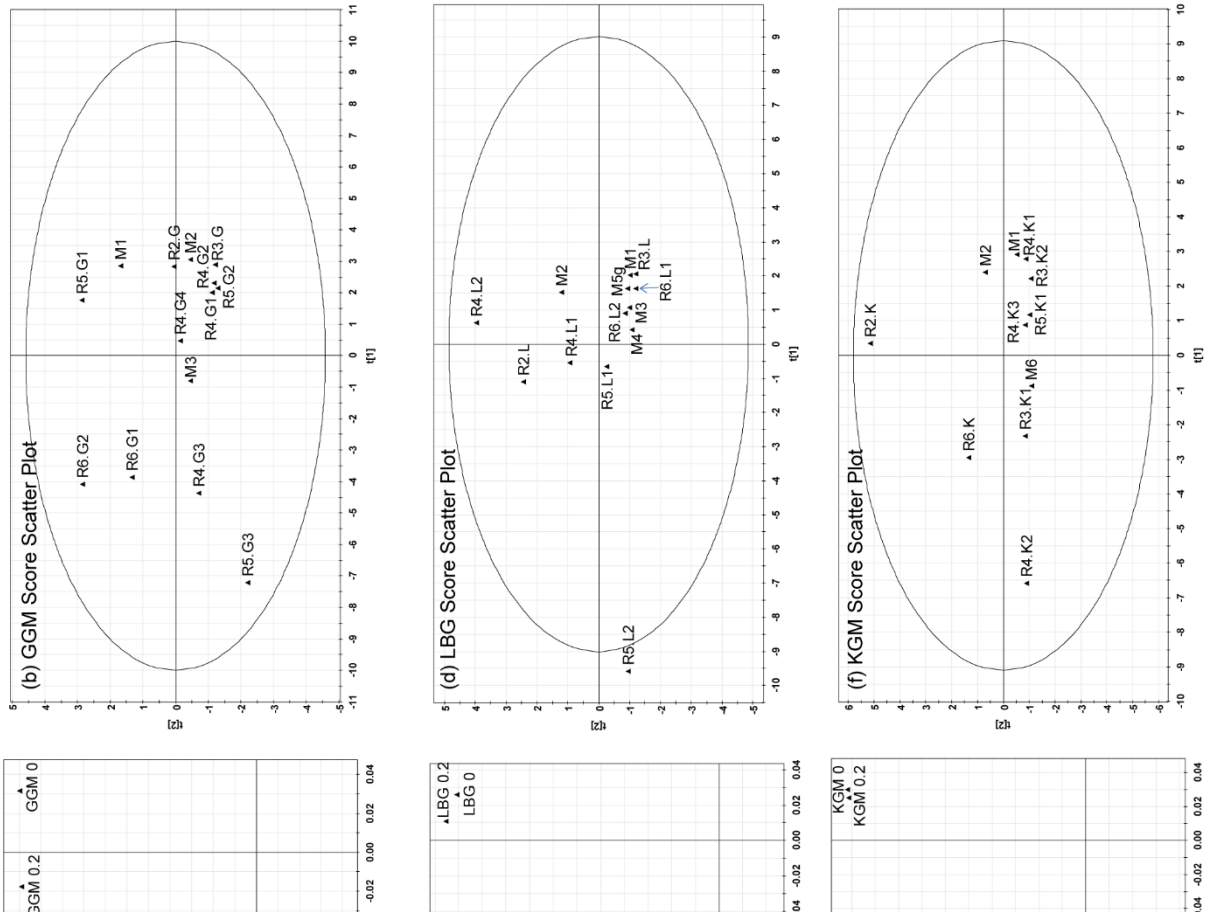

Fig. S12 PCA analysis of the oligomer spectrums. Plots are based on the first two principal components. These two components explain 74, 72, and 67 % of the variance for GGM, LBG and KGM, respectively. Names ending with ".2" represent duplicate samples.

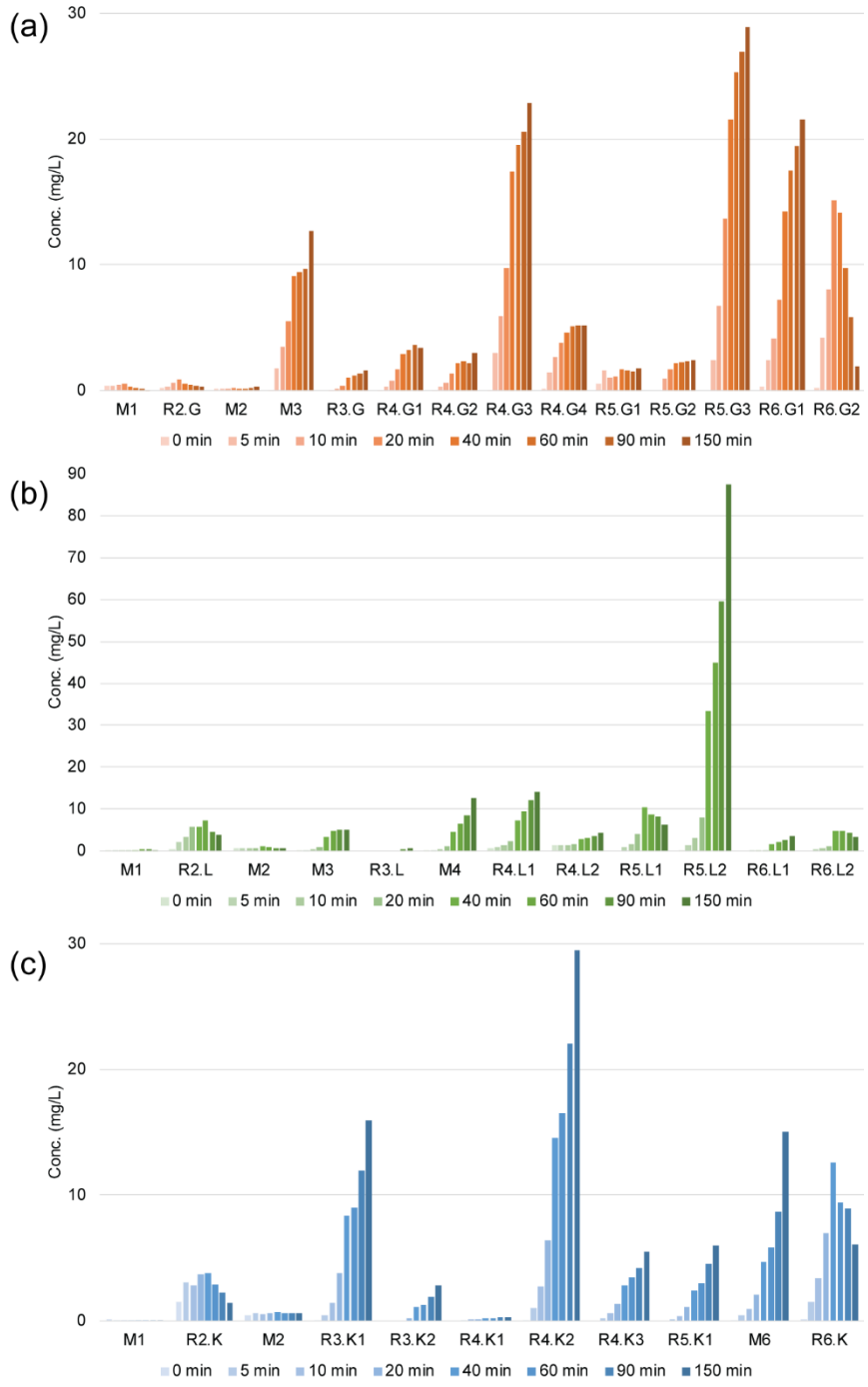

Fig. S13 Oligomer concentration for (a) GGM, (b) LBG, and (c) KGM.

Table S4 Probability for the conformation of ω_{Gal} in (%).

	MMMM	MGMM	MMLM	MGLM	MLLM	MLLM
gt 300K	20	20	7	8	6	25
tg 300K	25	20	18	7	13	24
gg 300K	55	60	75	85	81	51
gt 366K	23	22	10	12	8	25
tg 366K	29	24	21	12	17	26
gg 366K	49	53	70	75	75	49

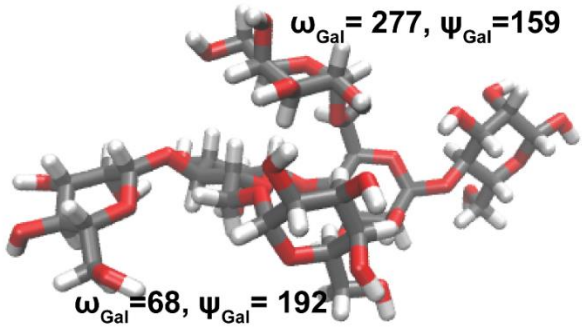

Fig. S14 Snapshot of MLLM oligomer.

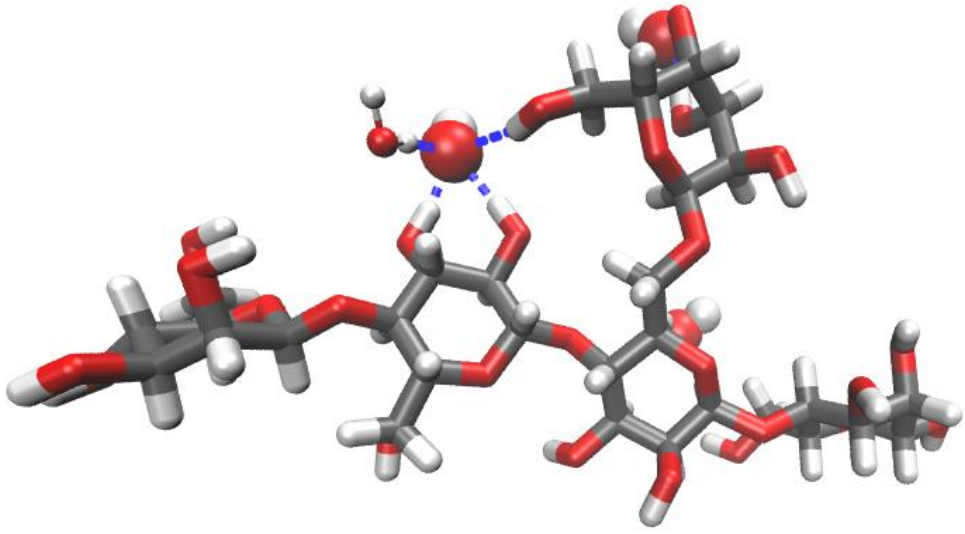

Fig. S15 Snapshot from the simulation showing OH^--coordination by Glc, Gal and one water molecule.

References

Hannuksela, T., & Hervé du Penhoat, C. (2004). NMR structural determination of dissolved O-acetylated galactoglucomannan isolated from spruce thermomechanical pulp. *Carbohydr. Res., 339*, 301-312.

Hub, J. S., Wolf, M. G., Caleman, C., van Maaren, P. J., Groenhof, G., & van der Spoel, D. (2014). Thermodynamics of hydronium and hydroxide surface solvation. *Chem. Sci., 5*, 1745-1749.

Malhotra, S. L. (1986). Ultrasonic Solution Degradations of Poly(Alkyl Methacrylates). *J. Macromol. Sci.-Chem., A23*, 729-748.

McLain, S., Imberti, S., Soper, A., Botti, A., Bruni, F., & Ricci, M. (2006). Structure of 2 molar NaOH in aqueous solution from neutron diffraction and empirical potential structural refinement. *Phys. Rev. B, 74*, 094201.

Pu, Y., Zou, Q., Hou, D., Zhang, Y., & Chen, S. (2017). Molecular weight kinetics and chain scission models for dextranpolymers during ultrasonic degradation. *Carbohydr. Polym., 156*, 71-76.

Wolf, M. G., Grubmüller, H., & Groenhof, G. (2014). Anomalous surface diffusion of protons on lipid membranes. *Biophys. J., 107*, 76-87.